Science Advances
AAAS

Supplementary Materials for

Heterojunction structures for reduced noise in large-area and sensitive perovskite x-ray detectors

Ying Zhou, Liang Zhao, Zhenyi Ni, Shuang Xu, Jingjing Zhao, Xun Xiao, Jinsong Huang*

*Corresponding author. Email: jhuang@unc.edu

Published 1 September 2021, *Sci. Adv.* **7**, eabg6716 (2021)
DOI: 10.1126/sciadv.abg6716

This PDF file includes:

Supplementary Text

Solar Cell Capacitance Simulator (SCAPS) simulation: the simulated *J-V* curves of perovskite heterojunction devices were obtained by using the Solar Cell Capacitance Simulator (SCAPS)(*42*). A basic planar structure of metal/perovskite/C_{60}/metal was constructed for the simulations. The basic parameters of each layer for the simulations of the *J-V* curves with the SCAPS package are shown in Table S1 and S2.

Halide ion diffusion simulation: Considering the ion diffuse in one direction in our heterojunction device, one dimensional partial diffusion equation in the form of $\frac{\partial u}{\partial t} = D\frac{\partial^2 u}{\partial x^2}$ was employed for Br diffusion simulation. In the specific simulation, the diffusion coefficient was set as measured Br/I interdiffusion coefficient of 2.6×10^{-12} cm^2 s^{-1} at room temperature(*37*), and the time was simulated to the 15th year. The total thickness in x direction is 500 µm. The initial condition is $u|_{0\le x\le 100} = 0.85$, and $u|_{100\le x\le 500} = 0$. The boundary conditions are set as $\frac{\partial u}{\partial x}|_{x=0} = 0$ and $\frac{\partial u}{\partial x}|_{x=500} = 0$, meaning there is no Br^- ions flux in or out at the top and bottom interfaces. MATLAB was used to simulation the diffusion process.

Table S1 Basic parameters of each layer for the simulations of perovskite heterojunction devices with the SCAPS package.

	Composition 1	**Composition 2**	**C_{60}**
Thickness (μm)	400	100	0.1
Bandgap (eV)	1.52	2.04	1.90
Electron affinity (eV)	4.00	3.48	4.10
Dielectric permittivity (relative)	31.00	31.00	5.00
CB effective DOS (1/cm^3)	2.00E18	2.00E18	2.00E18
VB effective DOS (1/cm^3)	2.00E18	2.00E18	2.00E18
Electron thermal velocity (cm/s)	1.00E7	1.00E7	1.00E7
Hole thermal velocity (cm/s)	1.00E7	1.00E7	1.00E7
Electron mobility (cm^2/Vs)	0.1	10.00	0.01
Hole mobility (cm^2/Vs)	0.1	10.00	0.01
Shallow donor density ND (1/cm^3)	1.00E10	1.00E10	1.00E12
Shallow acceptor density NA (1/cm^3)	1.00E9	1.00E10	0.00

Table S2 Basic parameters of the graded perovskite layer for the simulations of perovskite heterojunction devices with the SCAPS package.

	Graded perovskite	
Thickness (μm)	500	
Grading functional	Beta function, a = 4.0, b = 3.0	
	C_{60} side	**Metal side**
Bandgap (eV)	1.53	1.74
Electron affinity (eV)	3.99	3.78
Dielectric permittivity (relative)	31.00	31.00
CB effective DOS (1/cm^3)	2.00E18	2.00E18
VB effective DOS (1/cm^3)	2.00E18	2.00E18
Electron thermal velocity (cm/s)	1.00E7	1.00E7
Hole thermal velocity (cm/s)	1.00E7	1.00E7
Electron mobility (cm^2/Vs)	0.1	10
Hole mobility (cm^2/Vs)	0.1	10
Shallow donor density ND (1/cm^3)	1.00E10	1.00E10
Shallow acceptor density NA (1/cm^3)	1.00E9	1.00E10

Table S3 Work function and VBM position of $Cs_{0.15}FA_{0.85}PbI_3$ and $Cs_{0.15}FA_{0.85}Pb(I_{0.15}Br_{0.85})_3$.

	Work function (eV)	VBM (eV)
$Cs_{0.15}FA_{0.85}PbI_3$	5.23	-6.12
$Cs_{0.15}FA_{0.85}Pb(I_{0.15}Br_{0.85})_3$	5.22	-6.14

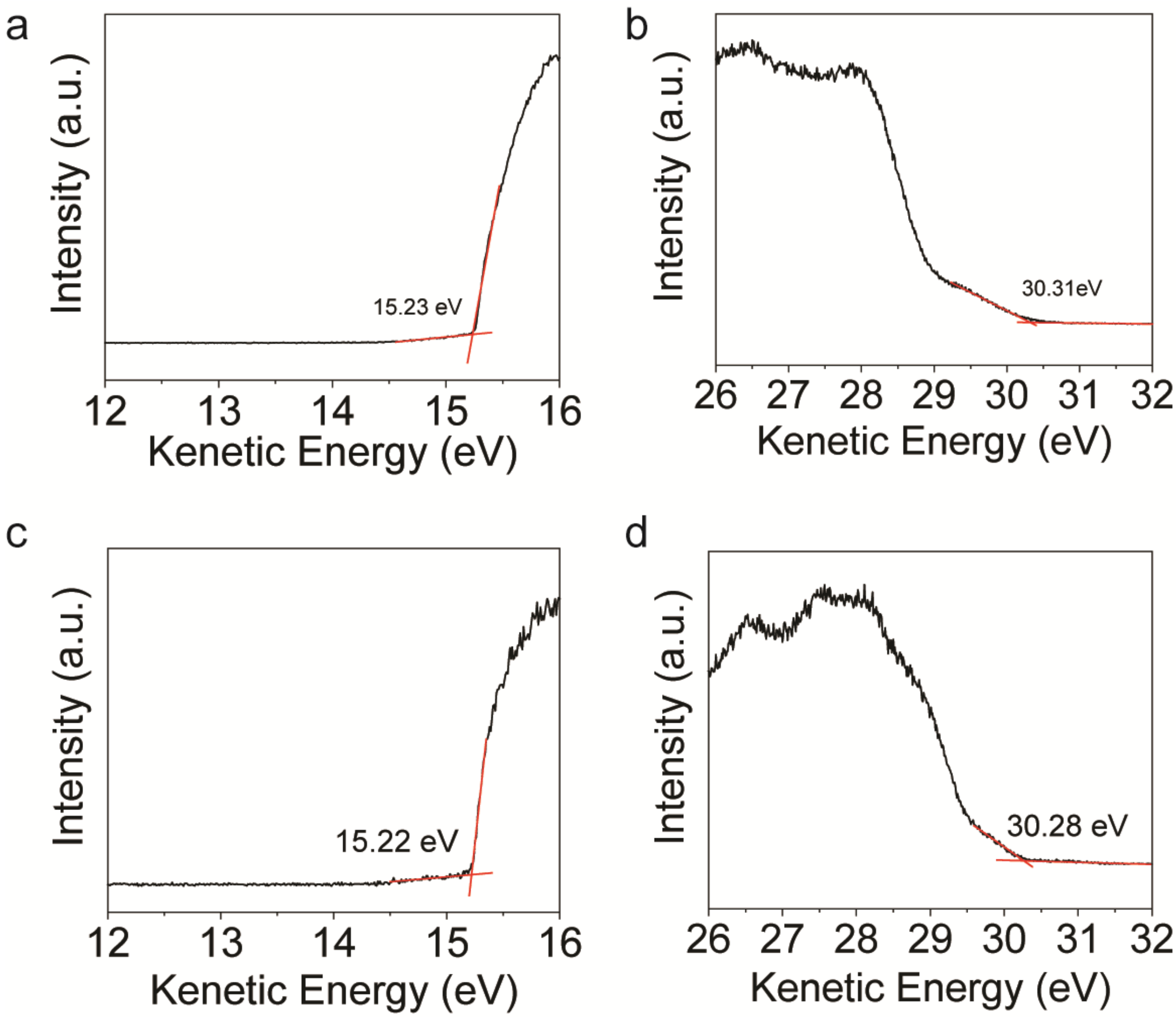

Fig. S1. Ultraviolet photoelectron spectroscopy of $Cs_{0.15}FA_{0.85}PbI_3$ and $Cs_{0.15}FA_{0.85}Pb(I_{0.15}Br_{0.85})_3$. Work function and VBM edge of $Cs_{0.15}FA_{0.85}PbI_3$ (**A**, **B**) and $Cs_{0.15}FA_{0.85}Pb(I_{0.15}Br_{0.85})_3$ (**C**, **D**). The energy of the UV source (He I) is 21.2 eV, and the samples were biased at 10 V during measurement.

Fig. S2. Photograph of partly peeled-off laminated heterojunction perovskite film. Photo Credit: Ying Zhou, University of North Carolina at Chapel Hill.

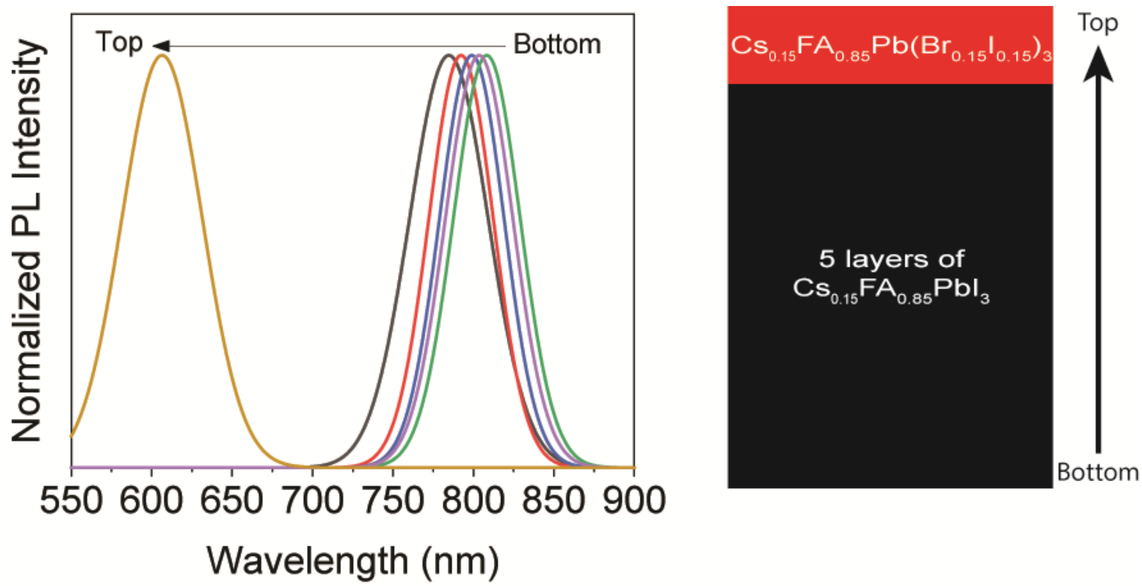

Fig. S3. Location dependent photoluminescence. The laminated heterojunction perovskite film was peeled off layer by layer, and characterized by PL with an excitation wavelength of 485 nm.

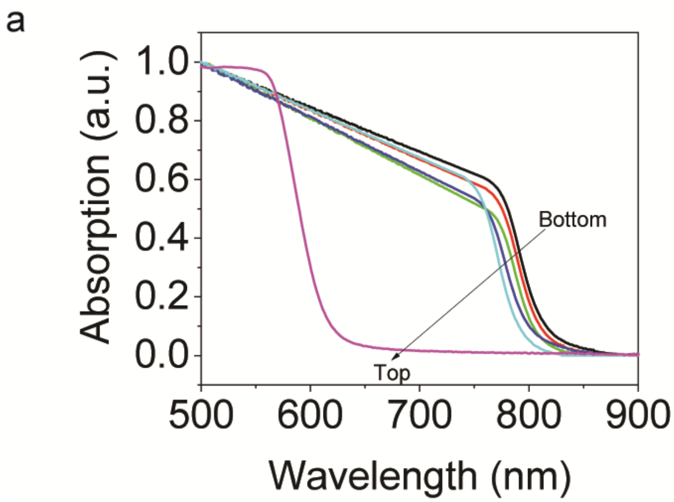

Fig. S4. Bandgap characterized by UV-Vis. UV-Vis spectra of the films peeled off layer by layer from the bottom $Cs_{0.15}FA_{0.85}PbI_3$ layer to the top $Cs_{0.15}FA_{0.85}Pb(I_{0.15}Br_{0.85})_3$ layer.

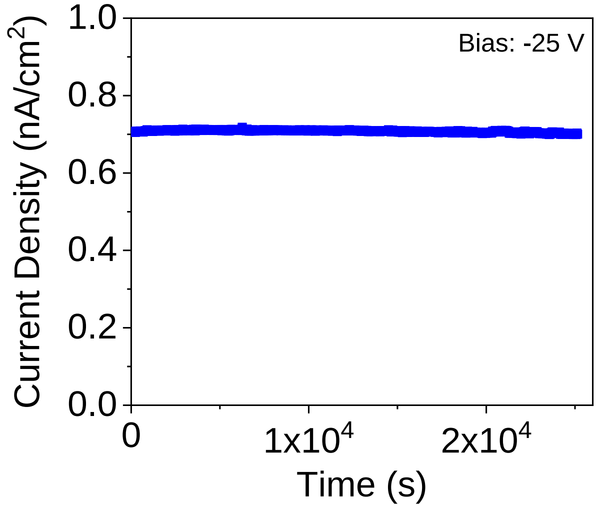

Fig. S5. Dark current monitor under a bias of -25 V for 7 hours.

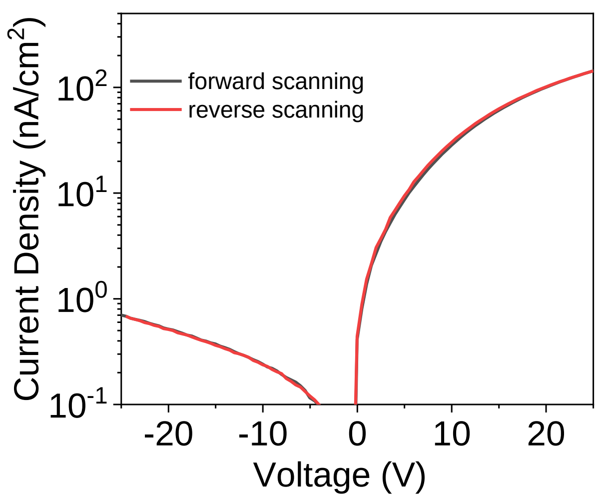

Fig. S6. Hysteresis characterization of heterojunction device. Forward and reverse scanning *J*-*V* curves of the heterojunction device were carried out using a scanning speed of 0.5 V every 3 seconds per step**.**

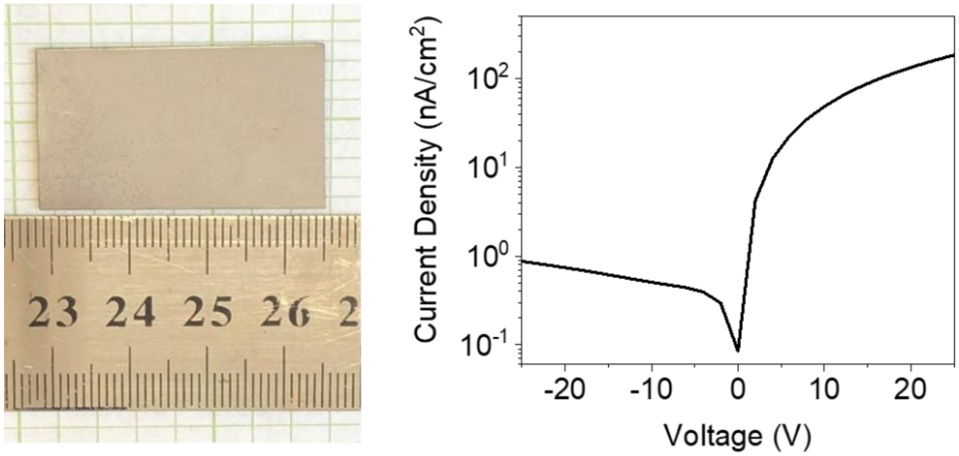

Fig. S7. Large area heterojunction device dark current. A heterojunction detector with an area of 7.92 cm^2 (2.2 cm×3.6 cm) was fabricated, and its *J-V* curve in the dark. The dark current density was 0.863 nA cm^{-2} at a bias of -25V. Photo Credit: Ying Zhou, University of North Carolina at Chapel Hill.

REFERENCES AND NOTES

1. H. Wei, Y. Fang, P. Mulligan, W. Chuirazzi, H.-H. Fang, C. Wang, B. R. Ecker, Y. Gao, M. A. Loi, L. Cao, J. Huang, Sensitive x-ray detectors made of methylammonium lead tribromide perovskite single crystals. *Nat. Photonics* **10**, 333–339 (2016).

2. Q. Dong, Y. Fang, Y. Shao, P. Mulligan, J. Qiu, L. Cao, J. Huang, Electron-hole diffusion lengths > 175 µm in solution-grown $CH_3NH_3PbI_3$ single crystals. *Science* **347**, 967–970 (2015).

3. H. Wei, D. DeSantis, W. Wei, Y. Deng, D. Guo, T. J. Savenije, L. Cao, J. Huang, Dopant compensation in alloyed $CH_3NH_3PbBr_{3-x}Cl_x$ perovskite single crystals for gamma-ray spectroscopy. *Nat. Mater.* **16**, 826–833 (2017).

4. Y. Fang, Q. Dong, Y. Shao, Y. Yuan, J. Huang, Highly narrowband perovskite single-crystal photodetectors enabled by surface-charge recombination. *Nat. Photonics* **9**, 679–686 (2015).

5. D. Shi, V. Adinolfi, R. Comin, M. Yuan, E. Alarousu, A. Buin, Y. Chen, S. Hoogland, A. Rothenberger, K. Katsiev, Y. Losovyj, X. Zhang, P. A. Dowben, O. F. Mohammed, E. H. Sargent, O. M. Bakr, Low trap-state density and long carrier diffusion in organolead trihalide perovskite single crystals. *Science* **347**, 519–522 (2015).

6. Z. Ni, C. Bao, Y. Liu, Q. Jiang, W.-Q. Wu, S. Chen, X. Dai, B. Chen, B. Hartweg, Z. Yu, Z. Holman, J. Huang, Resolving spatial and energetic distributions of trap states in metal halide perovskite solar cells. *Science* **367**, 1352–1358 (2020).

7. Q. Chen, J. Wu, X. Ou, B. Huang, J. Almutlaq, A. A. Zhumekenov, X. Guan, S. Han, L. Liang, Z. Yi, J. Li, X. Xie, Y. Wang, Y. Li, D. Fan, D. B. L. Teh, A. H. All, O. F. Mohammed, O. M. Bakr, T. Wu, M. Bettinelli, H. Yang, W. Huang, X. Liu, All-inorganic perovskite nanocrystal scintillators. *Nature* **561**, 88–93 (2018).

8. M. Gandini, I. Villa, M. Beretta, C. Gotti, M. Imran, F. Carulli, E. Fantuzzi, M. Sassi, M. Zaffalon, C. Brofferio, L. Manna, L. Beverina, A. Vedda, M. Fasoli, L. Gironi, S. Brovelli, Efficient, fast and reabsorption-free perovskite nanocrystal-based sensitized plastic scintillators. *Nat. Nanotechnol.* **15**, 462–468 (2020).

9. Y. Liu, X. Zheng, Y. Fang, Y. Zhou, Z. Ni, X. Xiao, S. Chen, J. Huang, Ligand assisted growth of perovskite single crystals with low defect density. *Nat. Commun.* **12**, 1686 (2021).

10. W. Wei, Y. Zhang, Q. Xu, H. Wei, Y. Fang, Q. Wang, Y. Deng, T. Li, A. Gruverman, L. Cao, J. Huang, Monolithic integration of hybrid perovskite single crystals with heterogenous substrate for highly sensitive x-ray imaging. *Nat. Photonics* **11**, 315–321 (2017).

11. G. Spekowius, T. Wendler, *Advances in Healthcare Technology: Shaping the Future of Medical Care* (Springer Science & Business Media, 2006), vol. 6.

12. A. Smith, Fundamentals of digital mammography: Physics, technology and practical considerations. *Radiol. Manag.* **25 5**, 18–24, 26–31; quiz 32–14 (2003).

13. H. Wei, J. Huang, Halide lead perovskites for ionizing radiation detection. *Nat. Commun.* **10**, 1066 (2019).

14. R. Zhuang, X. Wang, W. Ma, Y. Wu, X. Chen, L. Tang, H. Zhu, J. Liu, L. Wu, W. Zhou, X. Liu, Y. Yang, Highly sensitive x-ray detector made of layered perovskite-like $(NH_4)_3Bi_2I_9$ single crystal with anisotropic response. *Nat. Photonics* **13**, 602–608 (2019).

15. W. Pan, H. Wu, J. Luo, Z. Deng, C. Ge, C. Chen, X. Jiang, W.-J. Yin, G. Niu, L. Zhu, L. Yin, Y. Zhou, Q. Xie, X. Ke, M. Sui, J. Tang, $Cs_2AgBiBr_6$ single-crystal x-ray detectors with a low detection limit. *Nat. Photonics* **11**, 726–732 (2017).

16. B. Yang, W. Pan, H. Wu, G. Niu, J.-H. Yuan, K.-H. Xue, L. Yin, X. Du, X.-S. Miao, X. Yang, Q. Xie, J. Tang, Heteroepitaxial passivation of $Cs_2AgBiBr_6$ wafers with suppressed ionic migration for x-ray

imaging. *Nat. Commun.* **10**, 1989 (2019).

17. Y. Fang, A. Armin, P. Meredith, J. Huang, Accurate characterization of next-generation thin-film photodetectors. *Nat. Photonics* **13**, 1–4 (2019).

18. J. Zhao, L. Zhao, Y. Deng, X. Xiao, Z. Ni, S. Xu, J. Huang, Perovskite-filled membranes for flexible and large-area direct-conversion x-ray detector arrays. *Nat. Photonics* **14**, 612–617 (2020).

19. H. Huang, S. Abbaszadeh, Recent developments of amorphous selenium-based X-Ray detectors: A review. *IEEE Sensors J.* **20**, 1694–1704 (2020).

20. J. R. Scheuermann, A. H. Goldan, O. Tousignant, S. Léveillé, W. Zhao, Development of solid-state avalanche amorphous selenium for medical imaging. *Med. Phys.* **42**, 1223–1226 (2015).

21. D. M. Hunter, G. Belev, S. Kasap, M. J. Yaffe, Measured and calculated K-fluorescence effects on the MTF of an amorphous-selenium based CCD x-ray detector. *Med. Phys.* **39**, 608–622 (2012).

22. H. Li, J. Song, W. Pan, D. Xu, W.-a. Zhu, H. Wei, B. Yang, Sensitive and stable 2D perovskite single-crystal x-ray detectors enabled by a supramolecular anchor. *Adv. Mater.* **32**, 2003790 (2020).

23. S. Kasap, J. B. Frey, G. Belev, O. Tousignant, H. Mani, J. Greenspan, L. Laperriere, O. Bubon, A. Reznik, G. De Crescenzo, K. S. Karim, J. A. Rowlands, Amorphous and polycrystalline photoconductors for direct conversion flat panel x-ray image sensors. *Sensors* **11**, 5112–5157 (2011).

24. Y. Deng, C. H. Van Brackle, X. Dai, J. Zhao, B. Chen, J. Huang, Tailoring solvent coordination for high-speed, room-temperature blading of perovskite photovoltaic films. *Sci. Adv.* **5**, eaax7537 (2019).

25. Y. C. Kim, K. H. Kim, D.-Y. Son, D.-N. Jeong, J.-Y. Seo, Y. S. Choi, I. T. Han, S. Y. Lee, N.-G. Park, Printable organometallic perovskite enables large-area, low-dose x-ray imaging. *Nature* **550**, 87–91 (2017).

26. S. Shrestha, R. Fischer, G. J. Matt, P. Feldner, T. Michel, A. Osvet, I. Levchuk, B. Merle, S. Golkar, H. Chen, S. F. Tedde, O. Schmidt, R. Hock, M. Rührig, M. Göken, W. Heiss, G. Anton, C. J. Brabec, High-performance direct conversion x-ray detectors based on sintered hybrid lead triiodide perovskite wafers. *Nat. Photonics* **11**, 436–440 (2017).

27. W. Pan, B. Yang, G. Niu, K. H. Xue, X. Du, L. Yin, M. Zhang, H. Wu, X. S. Miao, J. Tang, Hot-pressed $CsPbBr_3$ quasi-Mmonocrystalline film for sensitive direct x-ray detection. *Adv. Mater.* **31**, 1904405 (2019).

28. D. J. Brenner, C. D. Elliston, E. J. Hall, W. E. Berdon, Estimated risks of radiation-induced fatal cancer from pediatric CT. *Am. J. Roentgenol.* **176**, 289–296 (2001).

29. J.-P. Moy, Recent developments in x-ray imaging detectors. *Nucl. Instrum. Methods Phys. Res. B* **442**, 26–37 (2000).

30. H. Wei, S. Chen, J. Zhao, Z. Yu, J. Huang, Is formamidinium always more stable than methylammonium? *Chem. Mater.* **32**, 2501–2507 (2020).

31. A. Mei, X. Li, L. Liu, Z. Ku, T. Liu, Y. Rong, M. Xu, M. Hu, J. Chen, Y. Yang, M. Grätzel, H. Han, A hole-conductor–free, fully printable mesoscopic perovskite solar cell with high stability. *Science* **345**, 295–298 (2014).

32. J. Androulakis, S. C. Peter, H. Li, C. D. Malliakas, J. A. Peters, Z. Liu, B. W. Wessels, J.-H. Song, H. Jin, A. J. Freeman, M. G. Kanatzidis, Dimensional reduction: A design tool for new radiation detection materials. *Adv. Mater.* **23**, 4163–4167 (2011).

33. G. Zentai, L. D. Partain, R. Pavlyuchkova, C. Proano, G. F. Virshup, B. N. Breen, A. I. Vilensky, O. Dagan, E. Meerson, M. Schieber, in *Smart Nondestructive Evaluation and Health Monitoring of Structural and Biological Systems II* (International Society for Optics and Photonics, 2003), vol. 5047, pp. 84–95.

34. P. Sprawls, *Physical Principles of Medical Imaging* (Aspen Publishers Gaithersburg, 1993).

35. D. Hart, M. Hillier, P. Shrimpton, Doses to patients from radiographic and fluoroscopic x-ray imaging procedures in the UK-2010 review. HPA-CRCE-034. *Health Protection Agency*, (2012).

36. Y. Yuan, J. Huang, Ion migration in organometal trihalide perovskite and its impact on photovoltaic efficiency and stability. *Acc. Chem. Res.* **49**, 286–293 (2016).

37. A. Osherov, Y. Feldman, I. Kaplan-Ashiri, D. Cahen, G. Hodes, Halide diffusion in $MAPbX_3$: Limits to topotaxy for halide exchange in perovskites. *Chem. Mater.* **32**, 4223–4231 (2020).

38. A. A. Zhumekenov, M. I. Saidaminov, M. A. Haque, E. Alarousu, S. P. Sarmah, B. Murali, I. Dursun, X.-H. Miao, A. L. Abdelhady, T. Wu, O. F. Mohammed, O. M. Bakr, Formamidinium lead halide perovskite crystals with unprecedented long carrier dynamics and diffusion length. *ACS Energy Lett.* **1**, 32–37 (2016).

39. K. T. Cho, S. Paek, G. Grancini, C. Roldán-Carmona, P. Gao, Y. Lee, M. K. Nazeeruddin, Highly efficient perovskite solar cells with a compositionally engineered perovskite/hole transporting material interface. *Energy Environ. Sci.* **10**, 621–627 (2017).

40. N. Li, Y. Luo, Z. Chen, X. Niu, X. Zhang, J. Lu, R. Kumar, J. Jiang, H. Liu, X. Guo, B. Lai, G. Brocks, Q. Chen, S. Tao, D. P. Fenning, H. Zhou, Microscopic degradation in formamidinium-cesium lead iodide perovskite solar cells under operational stressors. *Joule* **4**, 1743–1758 (2020).

41. Z. Muhammad, P. Liu, R. Ahmad, S. J. Asadabadi, C. Franchini, I. Ahmad, Tunable relativistic quasiparticle electronic and excitonic behavior of the $FAPb(I_{1-x}Br_x)_3$ alloy. *Phys. Chem. Chem. Phys.* **22**, 11943–11955 (2020).

42. M. Burgelman, P. Nollet, S. Degrave, Modelling polycrystalline semiconductor solar cells. *Thin Solid Films* **361**, 527–532 (2000).